Itinerant Microwave Photon Detector

Baptiste Royer,[1,*] Arne L. Grimsmo,[1,2] Alexandre Choquette-Poitevin,[1] and Alexandre Blais[1,3]

[1]*Institut quantique and Départment de Physique, Université de Sherbrooke,*
2500 boulevard de l'Université, Sherbrooke, Québec J1K 2R1, Canada
[2]*Centre for Engineered Quantum Systems, School of Physics, The University of Sydney, Sydney, New South Wales 2006, Australia*
[3]*Canadian Institute for Advanced Research, Toronto, Ontario M5G 1Z8, Canada*

The realization of a high-efficiency microwave single photon detector is a long-standing problem in the field of microwave quantum optics. Here, we propose a quantum nondemolition, high-efficiency photon detector that can readily be implemented in present state-of-the-art circuit quantum electrodynamics. This scheme works in a continuous fashion, gaining information about the photon arrival time as well as about its presence. The key insight that allows us to circumvent the usual limitations imposed by measurement backaction is the use of long-lived dark states in a small ensemble of inhomogeneous artificial atoms to increase the interaction time between the photon and the measurement device. Using realistic system parameters, we show that large detection fidelities are possible.

Introduction.—While the detection of localized microwave photons has been realized experimentally [1–3], high-efficiency detection of single *itinerant* microwave photons remains an elusive task [4]. Such detectors are increasingly sought after due to their applications in quantum information processing [5–7], microwave quantum optics [8], quantum radars [9–11], and even the detection of dark matter axions [12].

In recent years, a large number of microwave photon detector proposals have been put forward [13–21], and some proof-of-principle experiments have been performed [7,22–24]. For their operation, many of these proposals rely on *a priori* information about the photon arrival time [7,14,15,17,24,25], limiting their applicability. In this Letter, we are rather interested in continuous detectors, where the arrival time of a photon can be inferred *a posteriori* [13,16,18–23]. Moreover, we also focus on nondestructive detection of photons [4,13,19,25]. This property proves to be useful in a number of applications, such as quantum networks [5,6] and the study of quantum measurement [26]. A challenge in designing continuous single photon detectors is set by the quantum Zeno effect, which loosely states that the more strongly a quantum system is measured the less likely it is to change its state [27–29]. Any nonheralded photon detection scheme based on absorbing the photon into a medium thus faces the problem that strong continuous measurement reduces the absorption efficiency and thus the photon detection efficiency [13].

In this Letter, we introduce a nondestructive and continuous microwave photon detector that circumvents this measurement backaction problem with minimal device complexity, without requiring any active control pulses, and avoiding the use of nonreciprocal elements [19,20]. In essence, our proposal relies on absorbing a signal photon in a medium made of an ensemble of inhomogeneous artificial atoms, where the presence of long-lived dark states allows us to increase the effective lifetime of photons inside this composite absorber without lowering its bandwidth. We show that high detection efficiencies can be obtained by weakly and continuously monitoring the ensemble excitation number. We also present a simple circuit-QED design implementing this idea [30,31], where an ensemble of transmon qubits [32] are continuously measured through standard dispersive measurement.

Single-absorber detector.—Before introducing our proposal based on an ensemble of artificial atoms, we first study a simple single-absorber model and motivate our solution by explaining how the quantum efficiency of such a scheme is fundamentally limited due to quantum mechanical backaction effects. This simple model is illustrated in Fig. 1(a), where a signal photon (red) traveling along an input waveguide is absorbed into a single "absorber" mode B (orange) at a rate κ_B. This first mode is coupled to a second "measurement" harmonic mode A (green) which decays at a rate κ_A into an output port continuously measured using a standard homodyne measurement chain (not shown). In this toy model, we assume that the two modes are coupled by the longitudinal interaction ($\hbar = 1$),

$$\hat{H}_I = g_z \hat{b}^\dagger \hat{b}(\hat{a} + \hat{a}^\dagger), \tag{1}$$

where $\hat{a}$ and $\hat{b}$ are the annihilation operators of modes A and B, respectively. This interaction implements a textbook photon number measurement: the measured observable $\hat{b}^\dagger \hat{b}$ is coupled to the generator of displacement of a pointer
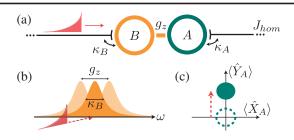
FIG. 1. (a) Sketch of a single absorber model for photon detection. A signal photon (red) is absorbed in a mode B and induces a coherent state displacement in a harmonic mode A which is measured using homodyne measurement. (b) Coupling between A and B induces fluctuations in the absorption spectrum of mode B, preventing the absorption of incoming photons. (c) Illustration of phase space for mode A as a photon is absorbed in B.

state $\hat{X}_A = \hat{a} + \hat{a}^\dagger$. As schematically illustrated in Fig. 1(c), the homodyne measurement of the orthogonal quadrature $\hat{Y}_A = -i(\hat{a} - \hat{a}^\dagger)$ allows us to precisely measure the photon number *inside* the absorber mode B without destroying the photon.

In order to induce a displacement in mode A, a signal photon however needs to first enter mode B, an unlikely process at large coupling strengths g_z. Indeed, as schematically illustrated in Fig. 1(b), $\hat{H}_I$ induces quantum fluctuations of the absorber's frequency which can prevent it from absorbing the arriving photon. This quantum fluctuation-induced spectral mismatch can be interpreted as a quantum Zeno-like effect since the width of these fluctuations directly relates to the measurement strength through g_z [29]. In order to minimize this unwanted measurement backaction, the width of these fluctuations, compared with the absorber's linewidth g_z/κ_B, should ideally be minimized. On the other hand, the displacement of the measurement mode A, which is given roughly by g_z/κ_B as well, should be maximized to improve the detection efficiency [33]. The optimal quantum efficiency of this toy model is obtained by balancing these two conflicting requirements. Numerically, we find an optimal operating point at $g_z/\kappa_B = 1$, the smallest coupling strength for which the induced displacement is distinguishable from vacuum noise $\langle \hat{Y}_A^2 \rangle_{\text{vacuum}} = 1$.

Numerical Simulations.—To model the signal photon arriving at the detector, a source mode C is introduced, with a frequency matching the absorber mode B, $\omega_C = \omega_B$. To minimize reflection, we take the signal photon linewidth to be much smaller than the absorber's linewidth, $\kappa_C/\kappa_B = 0.1$. Following the experiments of Refs. [34,35], this mode is initialized with one excitation leading to a signal photon emission with an exponentially decaying waveform.

The quantum efficiency of this simple photon detector is calculated by simulating multiple realizations of the above scenario and computing the corresponding

homodyne current out of the measurement mode A. This is realized by numerically integrating the stochastic master equation [26],

$$d\rho = \mathcal{L}\rho dt + \sqrt{\eta_h \kappa_A} \mathcal{H}[-i\hat{a}]\rho dW,$$

$$\hat{H} = \hat{H}_I - \frac{i\sqrt{\kappa_B \kappa_C}}{2}(\hat{c}\hat{b}^\dagger - \hat{c}^\dagger \hat{b}), \qquad (2)$$

where $\hat{c}$ is the annihilation operator of the source mode C and $\mathcal{L}\bullet$ is the Linbladian superoperator $\mathcal{L}\bullet = -i[\hat{H}, \bullet] + \sum_j \mathcal{D}[\hat{L}_j]\bullet$ with $\hat{L}_1 = \sqrt{\kappa_A}\hat{a}$, $\hat{L}_2 = \sqrt{\kappa_B}\hat{b} + \sqrt{\kappa_C}\hat{c}$. The combination of the term coupling $\hat{c}$ and $\hat{b}$ in $\hat{H}$ and of the composite decay operator $\hat{L}_2$ assures that the output of mode C is cascaded to the input of mode B [36,37]. Moreover, η_h is the homodyne measurement chain efficiency, $\mathcal{D}[\hat{L}]\bullet = \hat{L}\bullet\hat{L}^\dagger - \frac{1}{2}\{\hat{L}^\dagger\hat{L}, \bullet\}$ is the dissipation superoperator, and $\mathcal{H}[\hat{a}]\bullet = \hat{a}\bullet + \bullet\hat{a}^\dagger - \langle\hat{a} + \hat{a}^\dagger\rangle\bullet$ is the homodyne measurement backaction superoperator. The Wiener process dW is a random variable with the statistical properties $E[dW] = 0$ and $E[dW^2] = dt$, where $E[\bullet]$ denotes an ensemble average. For each trajectory, the resulting homodyne current is given by $J_{\text{hom}}(t) = \sqrt{\eta_h \kappa_A}\langle\hat{Y}_A\rangle + dW/dt$ [26]. Here and below, we use $N_{\text{traj}} = 2000$ trajectories and, to focus solely on the characteristics of the photodetector itself, assume a perfect homodyne detection chain $\eta_h = 1$.

For each homodyne current realization, we consider a photon is detected if the convolution of the signal with a filter, $\bar{J}_{\text{hom}}(t) = J_{\text{hom}}(t) \circ f(t)$, exceeds a threshold value Y_{thr}. To give more weight to times where the signal is, on average, larger, we use $f(t) \propto \langle\hat{Y}_A(t)\rangle_{\text{ME}}$ computed by solving the standard unconditional master equation [20]. The quantum efficiency $\eta = N_{\text{click}}/N_{\text{traj}}$ is then computed, where N_{click} is the number of trajectories where a photon is detected [38]. Although with this model no prior information about the photon arrival time is needed, if this information is available, the measurement can be restricted to a time window of length τ_m. In that case, a better metric is the measurement fidelity $\mathcal{F} = \frac{1}{2}(\eta + 1 - \Gamma_{\text{dark}} \times \tau_m)$ [17,19], where Γ_{dark} is the dark count rate, i.e., the rate at which the detector "clicks" without a signal photon. To maximize the detector repetition rate, τ_m is set to the smallest value that maximizes the fidelity.

For the single absorber model with $g_z/\kappa_B = 1$ and $\kappa_A/\kappa_B = 0.2$, we obtain an efficiency of 79% with $\Gamma_{\text{dark}}/\kappa_B = 1.4 \times 10^{-3}$ and a fidelity of $\mathcal{F} = 82\%$ for a time window of $\kappa_B \tau_m = 125$. The detector dead time after a detection event is given by the reset time of the measurement mode A back to vacuum. This corresponds to several decay times $1/\kappa_A$ or, alternatively, can be sped up by using active reset approaches [39–41].

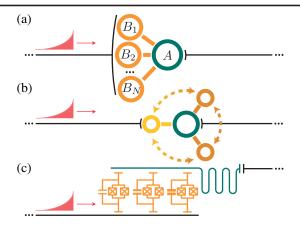This scheme is similar to previously studied models [13,20,42], and although it leads to relatively large

FIG. 2. (a) Absorber B is replaced by an ensemble of inhomogeneous modes coupled at the same point of the input waveguide. (b) Redrawing of (a) in the bright and dark states basis for $N = 3$. (c) Possible circuit-QED implementation for $N = 3$. Tunable transmon qubits acting as absorbers are coupled capacitively on one side to an input transmission line and on the other side to a measurement resonator.

detection fidelities, the resulting displacement of mode A is small, $\langle \hat{Y}_A \rangle \sim g_z / \kappa_B = 1$. In this situation, adding an imperfect homodyne measurement chain $\eta_h < 1$ leads to a significant reduction of the quantum efficiency.

Absorption into an ensemble.—As already pointed out, the key issue with using a single absorber is that both the total displacement of the measurement mode A and the measurement backaction on B scale with g_z / κ_B. This stems from the fact that the time spent in a simple resonant system is given by the inverse of its bandwidth. In order to increase the quantum efficiency, we thus present a scheme where the interaction time with the photon is increased while keeping the ratio g_z / κ_B constant.

As schematically illustrated in Fig. 2(a), we first replace the single absorber by a small ensemble of $N \lesssim 5$ artificial atoms, and second, we inhomogeneously detune each atom with respect to the average ensemble frequency. By connecting these absorbers approximately to the same point of the input waveguide [43], symmetry imposes that the absorbers state, after the absorption of a photon, should be invariant under permutation. The only state satisfying this condition is the all-symmetric superposition of excitation in the absorbers $\hat{b}_+ = 1/\sqrt{N}\sum_i \hat{b}_i$, which we refer to as the bright state [44,45]. Other nonsymmetric states, which we call dark states, completely decouple from the waveguide and are long lived. We, furthermore, design the coupling to the measurement mode A such that the measured observable is $\hat{N}_B = \sum_i \hat{b}_i^\dagger \hat{b}_i$, the total photon number in the ensemble. In this case, the ideal interaction picture Hamiltonian becomes

$$\hat{H}_I^E = g_z \hat{N}_B \hat{X}_A + \sum_{i=1}^{N} \Delta_i \hat{b}_i^\dagger \hat{b}_i, \qquad (3)$$

where $\Delta_i = \omega_{Bi} - \omega_B \lesssim \kappa_B$ is the ith atom detuning with respect to the average ensemble frequency $\omega_B = \sum_i \omega_{Bi}/N$, and the first term represents the direct generalization of Eq. (1) for an ensemble of atoms.

In this model, a signal photon is absorbed in the collective bright state $\hat{b}_+$ at a rate scaling linearly with N. Without loss of generality and to fix the effective collective absorption rate of the absorbers at κ_B, we choose the bare linewidth of the atoms to be $\kappa_{Bi} = \kappa_B/N$. In the case where the atoms are on resonance $\Delta_i = 0 \; \forall \; i$, the bright and dark subspaces are uncoupled, and the model becomes equivalent to the single absorber model illustrated in Fig. 1(a) [46].

On the other hand, nonhomogeneous detunings $\Delta_i \neq \Delta_j$ lead to coupling of the bright and dark subspaces. If this coupling is carefully adjusted, a signal photon can be absorbed into the bright state, transferred to a long-lived dark state, and after some time τ_{trap}, return to the bright state where it is re-emitted. Figure 2(b) illustrates this process schematically with the bright state (yellow) being coupled to $N - 1$ dark states (dark orange). In practice, this process is optimized by having equally spaced detunings. Crucially, changing the detunings affects neither the coupling strength g_z nor the effective linewidth κ_B, leaving the measurement backaction unaffected. On the other hand, the total displacement induced in the measurement mode A is changed from g_z / κ_B to roughly $g_z \times (1/\kappa_B + \tau_{\text{trap}})$. As a result, by increasing τ_{trap} and reducing g_z, we can thus, as desired, significantly increase the quantum efficiency by simultaneously increasing the induced displacement and reducing the measurement backaction. In practice, τ_{trap} can be made longer by increasing the number of dark states where the photon can get trapped (i.e., increasing N) and optimizing the detunings $\vec{\Delta}$ accordingly [47]. In the large N limit, the mechanism leading to τ_{trap} is reminiscent of photon memories using inhomogeneous spin ensembles [49–52].

We perform full stochastic master equation simulations using Eq. (2) with the replacements $\hat{b} \to \hat{b}_+$, $\hat{H}_I \to \hat{H}_I^E$ and show the increase in measurement fidelity $\mathcal{F}$ as a function of ensemble size in Fig. 3(a). As shown in Fig. 4(b), for $N = 4$, a quantum efficiency of $\eta = 92\%$ is obtained at a low estimated dark count rate $\Gamma_{\text{dark}}/\kappa_B = 7 \times 10^{-6}$. For a time window of $\kappa_B \tau_m = 126$, this translates to the measurement fidelity of $\mathcal{F} = 96\%$ observed in Fig. 4(a). As illustrated in Fig. 4(b), the threshold Y_{thr} can be varied to trade a higher dark count rate for a higher efficiency or the converse. Here, Γ_{dark} is computed from trajectories with no signal photon (full lines) and, where it is too small to be precisely calculated from trajectories, estimated from time correlations in the filtered signal from vacuum (colored dashed lines) [47].

Importantly, due to the increased interaction time, the measured homodyne signal increases with N and, for $N = 4$, is already much larger than vacuum noise. As a
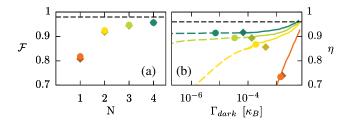
FIG. 3. (a) Fidelity as a function of the number of absorbers. The circles are calculated using the ideal model with $\kappa_A/\kappa_B = 0.2$, $g_z^{(1)}/\kappa_B = 1$, $g_z^{(2)}/\kappa_B = 0.6$, $g_z^{(3)}/\kappa_B = 0.5$, and $g_z^{(4)}/\kappa_B = 0.4$ with the detunings $\vec{\Delta}^{(2)}/\kappa_B = (0.55, -0.55)$, $\vec{\Delta}^{(3)}/\kappa_B = (0.7, -0.7, 0)$, and $\vec{\Delta}^{(4)}/\kappa_B = (0.7, -0.7, 0.23, -0.23)$. The diamonds are calculated using realistic parameters for a transmon ensemble dispersively coupled to a resonator with $\kappa_B/2\pi = 10$ MHz, $g_z/\chi = 10$, and T_1, $T_2 = 30$ μs. (b) Detector efficiency as a function of the dark count rate. Solid lines correspond to statistics extracted from trajectories, while for the dashed lines Γ_{dark} was estimated using an analytical formula. The lines were calculated for the ideal model, and the points indicate where the fidelity is maximized. The black dashed line in (a) and (b) correspond the upper bound $\eta_{\max}$ imposed by the photon shape used here.

result, the detector becomes increasingly robust to potential imperfections in the homodyne detection chain ($\eta_h < 1$). We, moreover, expect the quantum efficiency to continue increasing as the number of absorbers is raised above 4. For $N \geq 5$, the required Hilbert space size for numerical simulations is impractically large. Nevertheless, at $N = 4$, the performance is already close to an expected maximum of $\eta_{\max} \sim 96\%$ indicated by the black dashed line in Figs. 3(a) and 3(b). This upper bound is due to high frequency components of the signal photon that are directly reflected from the absorber and thus do not lead to a detectable signal in mode A [47]. This upper bound value is linked to the choice of both detector and signal photon parameters and could be improved upon further optimization.

Since our proposal is continuous, the time τ_c at which the homodyne signal crosses the threshold reveals information about the photon arrival time. Figure 4 shows histograms of the normalized number of counts for τ_c, as recorded from trajectories where a photon is detected. In Fig. 4(a), the number of absorbers is varied, and the signal threshold Y_{thr} is set to optimize the fidelity (see Fig. 3). On the other hand, in Fig. 4(b), we set $N = 4$ and vary the threshold. In both Figs. 4(a) and 4(b), the input photon shape (red) is shown for comparison. As the threshold increases, the distribution of crossing times narrows and the precision on the photon arrival time therefore increases. As mentioned above, increasing N leads to larger homodyne signals. Hence, adding more absorbers allows us to increase the threshold which, in turn, improves the arrival time precision. Moreover, since $1/\kappa_C$ is the longest timescale in these simulations, at $N = 4$ the photon shape can be resolved
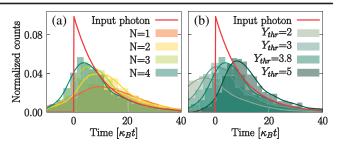

FIG. 4. (a) Normalized number of detection events as a function of time for (a) different number of absorbers in the ideal model Eq. (3) and for (b) different thresholds for $N = 4$. In both (a) and (b), the input photon shape (red) is shown for comparison and an arbitrary time offset has been substracted from the homodyne signal.

from the histogram. The mismatch between the distribution and the red line near $\kappa_B t = 0$ is due to the sharp, high frequency feature of the input photon that is reflected from the absorbers without detection.

Physical implementation.—A possible implementation of this model, based on dispersive coupling of transmon qubits, is illustrated in Fig. 2(c). Here, an ensemble of superconducting transmon qubits is capacitively coupled on one side to a transmission line and on the other side to a measurement resonator (mode A) with coupling strength g. We take a large detuning between the qubits center frequency ω_B and the resonator frequency $\omega_r - \omega_B \gg \kappa_A, \kappa_B, g$ and use the standard dispersive approximation [47]. The absorption of a signal photon by the qubits induces a shift in the resonator frequency which is detected by continuously probing the resonator with a coherent drive corresponding to a field amplitude α [30]. In this situation, we find that the system of Fig. 2(c) is well described by the displaced dispersive Hamiltonian [47],

$$\hat{H}_\chi^D = g_z \hat{N}_B \hat{X}_A + \sum_{i=1}^{N} \Delta_i \hat{b}_i^\dagger \hat{b}_i + 2\chi \hat{N}_B \hat{a}^\dagger \hat{a} + \Delta_+ \hat{b}_+^\dagger \hat{b}_+, \quad (4)$$

where χ is the usual transmon dispersive shift [32,47], $g_z = 2\chi\alpha$, and Δ_+ results from a combination of the resonator-induced Lamb shift and spurious qubit-qubit coupling [47]. The first two terms correspond exactly to the ideal model Hamiltonian Eq. (3), while the two additional last terms are small and imposed by this specific implementation.

As the diamonds in Fig. 3 show, at $\alpha = 5$, the two additional terms in Eq. (4) have a minimal impact on the quantum efficiency. Moreover, it is possible to mitigate the detrimental effect of a small Δ_+ by adjusting the detunings $\vec{\Delta}$.

As an example, choosing realistic parameters $N = 4$, $\kappa_B/2\pi = 10$ MHz, $\kappa_A/2\pi = 2$ MHz, $\chi/2\pi = 0.4$ MHz, $\alpha = 5$, and $\vec{\Delta}/2\pi = (6.6, -7.4, 2.3, -2.3)$ MHz and using current transmon decoherence times T_1, $T_2 = 30$ μs [53],

we obtain $\eta = 92\%$ with $\Gamma_{\text{dark}} = 4.2 \times 10^{-3} \ \mu\text{s}^{-1}$. Given a time window of $\tau_m = 2 \ \mu$s, this corresponds to a large measurement fidelity of $F = 96\%$.

Conclusion.—We have presented a high-efficiency, non-destructive scheme for itinerant microwave photon detection where no prior information about the photon arrival time is needed. This scheme is based on the continuous measurement of the photon number in an ensemble of inhomogeneous artificial atoms where the photon can be stored for long times due to the existence of long-lived dark states. We also presented a realistic physical implementation of this idea using an ensemble of transmon qubits dispersively coupled to a single resonator. Using only four transmons, we estimate that fidelities as high as 96% are attainable for the photon shape considered, and we expect that adding more transmons will improve this fidelity even further. Since the output signal is proportional to the total number of photons, the same model could be used as a photon-number resolving detector. Future work will investigate this possibility.

---

*baptiste.royer@usherbrooke.ca

[1] S. Gleyzes, S. Kuhr, C. Guerlin, J. Bernu, S. Deleglise, U. Busk Hoff, M. Brune, J.-M. Raimond, and S. Haroche, Nature (London) **446**, 297 (2007).

[2] B. R. Johnson, M. D. Reed, A. A. Houck, D. I. Schuster, L. S. Bishop, E. Ginossar, J. M. Gambetta, L. DiCarlo, L. Frunzio, S. M. Girvin, and R. J. Schoelkopf, Nat. Phys. **6**, 663 (2010).

[3] D. I. Schuster, A. A. Houck, J. A. Schreier, A. Wallraff, J. M. Gambetta, A. Blais, L. Frunzio, J. Majer, B. Johnson, M. H. Devoret, S. M. Girvin, and R. J. Schoelkopf, Nature (London) **445**, 515 (2007).

[4] S. R. Sathyamoorthy, T. M. Stace, and G. Johansson, C.R. Phys. **17**, 756 (2016).

[5] N. Gisin and R. Thew, Nat. Photonics **1**, 165 (2007).

[6] H. J. Kimble, Nature (London) **453**, 1023 (2008).

[7] A. Narla, S. Shankar, M. Hatridge, Z. Leghtas, K. M. Sliwa, E. Zalys-Geller, S. O. Mundhada, W. Pfaff, L. Frunzio, R. J. Schoelkopf, and M. H. Devoret, Phys. Rev. X **6**, 031036 (2016).

[8] C. Gardiner and P. Zoller, *Quantum Noise: A Handbook of Markovian and Non-Markovian Quantum Stochastic Methods with Applications to Quantum Optics*, Springer Series in Synergetics (Springer, New York, 2004).

[9] S. Lloyd, Science **321**, 1463 (2008).

[10] S.-H. Tan, B. I. Erkmen, V. Giovannetti, S. Guha, S. Lloyd, L. Maccone, S. Pirandola, and J. H. Shapiro, Phys. Rev. Lett. **101**, 253601 (2008).

[11] S. Guha and B. I. Erkmen, Phys. Rev. A **80**, 052310 (2009).

[12] S. K. Lamoreaux, K. A. van Bibber, K. W. Lehnert, and G. Carosi, Phys. Rev. D **88**, 035020 (2013).

[13] F. Helmer, M. Mariantoni, E. Solano, and F. Marquardt, Phys. Rev. A **79**, 052115 (2009).

[14] G. Romero, J. J. García-Ripoll, and E. Solano, Phys. Rev. Lett. **102**, 173602 (2009).

[15] C. H. Wong and M. G. Vavilov, Phys. Rev. A **95**, 012325 (2017).

[16] O. Kyriienko and A. S. Sørensen, Phys. Rev. Lett. **117**, 140503 (2016).

[17] K. Koshino, K. Inomata, T. Yamamoto, and Y. Nakamura, Phys. Rev. Lett. **111**, 153601 (2013).

[18] K. Koshino, Z. Lin, K. Inomata, T. Yamamoto, and Y. Nakamura, Phys. Rev. A **93**, 023824 (2016).

[19] S. R. Sathyamoorthy, L. Tornberg, A. F. Kockum, B. Q. Baragiola, J. Combes, C. M. Wilson, T. M. Stace, and G. Johansson, Phys. Rev. Lett. **112**, 093601 (2014).

[20] B. Fan, G. Johansson, J. Combes, G. J. Milburn, and T. M. Stace, Phys. Rev. B **90**, 035132 (2014).

[21] J. Leppäkangas, M. Marthaler, D. Hazra, S. Jebari, G. Johansson, and M. Hofheinz, Phys. Rev. A **97**, 013855 (2018).

[22] Y.-F. Chen, D. Hover, S. Sendelbach, L. Maurer, S. T. Merkel, E. J. Pritchett, F. K. Wilhelm, and R. McDermott, Phys. Rev. Lett. **107**, 217401 (2011).

[23] G. Oelsner, C. K. Andersen, M. Rehák, M. Schmelz, S. Anders, M. Grajcar, U. Hübner, K. Mølmer, and E. Il'ichev, Phys. Rev. Applied **7**, 014012 (2017).

[24] K. Inomata, Z. Lin, K. Koshino, W. D. Oliver, J.-S. Tsai, T. Yamamoto, and Y. Nakamura, Nat. Commun. **7**, 12303 (2016).

[25] A. Reiserer, S. Ritter, and G. Rempe, Science **342**, 1349 (2013).

[26] H. Wiseman and G. Milburn, *Quantum Measurement and Control* (Cambridge University Press, Cambridge, England, 2010).

[27] B. Misra and E. C. G. Sudarshan, J. Math. Phys. (N.Y.) **18**, 756 (1977).

[28] K. Kraus, Found. Phys. **11**, 547 (1981).

[29] P. Facchi and S. Pascazio, Phys. Rev. Lett. **89**, 080401 (2002).

[30] A. Blais, R.-S. Huang, A. Wallraff, S. M. Girvin, and R. J. Schoelkopf, Phys. Rev. A **69**, 062320 (2004).

[31] A. Wallraff, D. I. Schuster, A. Blais, L. Frunzio, R. S. Huang, J. Majer, S. Kumar, S. M. Girvin, and R. J. Schoelkopf, Nature (London) **431**, 162 (2004).

[32] J. Koch, T. M. Yu, J. Gambetta, A. A. Houck, D. I. Schuster, J. Majer, A. Blais, M. H. Devoret, S. M. Girvin, and R. J. Schoelkopf, Phys. Rev. A **76**, 042319 (2007).

[33] The displacement $\sim g_z/\kappa_B$ corresponds to the interaction strength multiplied by the typical photon lifetime inside B.

[34] A. A. Houck, D. I. Schuster, J. M. Gambetta, J. A. Schreier, B. R. Johnson, J. M. Chow, L. Frunzio, J. Majer, M. H. Devoret, S. M. Girvin, and R. J. Schoelkopf, Nature (London) **449**, 328 (2007).

[35] D. Bozyigit, C. Lang, L. Steffen, J. M. Fink, C. Eichler, M. Baur, R. Bianchetti, P. J. Leek, S. Filipp, M. P. da Silva, A. Blais, and A. Wallraff, Nat. Phys. **7**, 154 (2011).

[36] C. W. Gardiner, Phys. Rev. Lett. **70**, 2269 (1993).

[37] H. J. Carmichael, Phys. Rev. Lett. **70**, 2273 (1993).

[38] R. H. Hadfield, Nat. Photonics **3**, 696 (2009).

[39] D. T. McClure, H. Paik, L. S. Bishop, M. Steffen, J. M. Chow, and J. M. Gambetta, Phys. Rev. Applied **5**, 011001 (2016).

[40] C. C. Bultink, M. A. Rol, T. E. O'Brien, X. Fu, B. C. S. Dikken, C. Dickel, R. F. L. Vermeulen, J. C. de Sterke, A. Bruno, R. N. Schouten, and L. DiCarlo, Phys. Rev. Applied **6**, 034008 (2016).

[41] S. Boutin, C. K. Andersen, J. Venkatraman, A. J. Ferris, and A. Blais, Phys. Rev. A **96**, 042315 (2017).

[42] G. J. Milburn and S. Basiri-Esfahani, Proc. R. Soc. A **471**, 20150208 (2015).

[43] In practice, the distance d between the artificial atoms should be much smaller than their wavelength $d \ll 2\pi v_0/\omega_B$, with v_0 the speed of light in the waveguide and ω_B the atoms frequency.

[44] K. Lalumière, B. C. Sanders, A. F. van Loo, A. Fedorov, A. Wallraff, and A. Blais, Phys. Rev. A **88**, 043806 (2013).

[45] A. F. van Loo, A. Fedorov, K. Lalumière, B. C. Sanders, A. Blais, and A. Wallraff, Science **342**, 1494 (2013).

[46] B. Fan, A. F. Kockum, J. Combes, G. Johansson, I.-c. Hoi, C. M. Wilson, P. Delsing, G. J. Milburn, and T. M. Stace, Phys. Rev. Lett. **110**, 053601 (2013).

[47] See Supplemental Material at http://link.aps.org/supplemental/10.1103/PhysRevLett.120.203602 for more details on the analytical expressions and the simulations, which includes Ref. [48].

[48] U. Vool and M. Devoret, Int. J. Circuit Theory Appl. **45**, 897 (2017).

[49] Z. Kurucz, J. H. Wesenberg, and K. Mølmer, Phys. Rev. A **83**, 053852 (2011).

[50] I. Diniz, S. Portolan, R. Ferreira, J. M. Gérard, P. Bertet, and A. Auffèves, Phys. Rev. A **84**, 063810 (2011).

[51] Y. Kubo, I. Diniz, A. Dewes, V. Jacques, A. Dréau, J.-F. Roch, A. Auffeves, D. Vion, D. Esteve, and P. Bertet, Phys. Rev. A **85**, 012333 (2012).

[52] B. Julsgaard, C. Grezes, P. Bertet, and K. Mølmer, Phys. Rev. Lett. **110**, 250503 (2013).

[53] D. C. McKay, S. Filipp, A. Mezzacapo, E. Magesan, J. M. Chow, and J. M. Gambetta, Phys. Rev. Applied **6**, 064007 (2016).